Computers in Biology and Medicine 109 (2019) 91–100

Contents lists available at ScienceDirect

Computers in Biology and Medicine

journal homepage: www.elsevier.com/locate/compbiomed

The effect of chordae tendineae on systolic flow

John C. Morud*, Paal Skjetne, Stig Urheim, Sigrid K. Dahl

SINTEF Industry, Trondheim, Norway

ARTICLE INFO

Keywords:
Left ventricle
Chordae tendineae
Computational fluid dynamics
CFD
3D ultrasound
Patient-specific simulations

ABSTRACT

When using Computational Fluid Dynamics to simulate ventricular blood flow in the heart, it has been common practice to neglect the effect of the sub-valvular apparatus and the trabeculae on the flow conditions. In this study, we analyze the effect of neglecting the chordae tendineae on the fluid flow and pressure drop. To test the assumption we use a previously developed dynamic 3D model of the left ventricle, aorta and valves that is based on 3D echocardiographic recordings. To this model we add the chordae tendineae as a sub-grid model.

The previously developed 3D model for the left ventricle during systole is based on real-time three-dimensional echocardiography (RT3DE) recordings of a 30 years old female volunteer. The segmented ventricular wall does not include details of the aorta and the mitral valve, so these were reconstructed. The subgrid model for the flow across the chordae tendineae is based on the Actuator Line Method, which means that they are represented by drag coefficients. The analysis shows that the effect of the chordae tendineae on the pressure drop and work efficiency of the normal heart during systole is minor, and it seems that for simulating ventricular fluid flow and pressure drop during systole, one can follow the current practice and ignore the chordae. However, there can be local effects such as small vortices behind the chordae. Whether such effects are important for a particular application must be evaluated for the given case.

1. Introduction

The mitral valve (MV) apparatus of the human heart consists of two leaflets, the mitral annulus, the chordae tendineae and the papillary muscles (PM). The latter two are also referred to as the sub-valvular apparatus [1] which supports the mitral valve against the large pressure difference during ventricular systole. Thus, the chordae tendineae and the papillary muscles are required from a mechanical point of view for normal operation of the valve. Rupture of chords may lead to valve regurgitation and thus indirectly to unfavorable flow conditions.

When simulating blood flow using Computational Fluid Dynamics (CFD), it has been common practice to neglect the effect of the sub-valvular apparatus and the trabeculae on the flow conditions in the heart. The effect of this simplification on the flow field and pressure drop is then left as an open question, with the suggestion that it can have an effect on the flow [2–18]. However, there has been recent work on the trabeculae and papillary muscles in the literature, both in the left ventricle [19–24] and in the right ventricle [25]. In this study, the focus has been on the influence of the chordae tendineae on the flow, thus the papillary muscles and the trabecula have not been modeled. There are some recent articles who have included the chordae tendineae in their model [26–28]. These are fluid structure interaction (FSI) models and different approaches for calculating the flow equations have been used. Caballero et al. [26] and Singh-Gryzbon et al.[28] used a mesh free method called the Smoothed Particle Hydrodynamics (SPH) method. Meschini et al. [27] used a fixed grid method called the Immersed Boundary method, whereas our work is based on a moving grid method called the Arbitrary-LagrangianEulerian (ALE) method. The different methods have their advantages and drawbacks.

Intra-cardiac blood flow has been calculated by CFD as early as in 1977 by Peskin [29,30], who used an immersed boundary method to represent the moving heart walls. Basically this amounts to using momentum source terms to represent the moving solid walls. However, whereas this method is very flexible it is difficult to resolve flow details on realistic grids, especially close to the walls. Since then, there has been an enormous development both in computer power and in numerical techniques. A trend in academia has thus been towards extremely detailed simulations where small structures of the heart wall, papillary muscles and even the chordae tendineae are recorded using high-resolution CT and used to generate geometries for CFD and FSI simulations. Such high-fidelity simulations can then be used as a valuable supplement to experiments in fundamental studies in order to understand the flow and mechanics of the heart [20–22,24,31].

Whereas high-fidelity simulations are valuable for fundamental

* Corresponding author.
E-mail address: john.morud@sintef.no (J.C. Morud).

https://doi.org/10.1016/j.compbiomed.2019.04.020
Received 18 December 2018; Received in revised form 10 April 2019; Accepted 20 April 2019

studies, they have large costs both in terms of CPU usage and geometry recording by imaging. For practical clinical applications in the future it is thus desirable to strive for simplification of the geometry and develop CFD models that have lower setup- and computational costs. In the present work we make a trade-off: The geometry of the ventricular wall, aorta and mitral valve is represented by means of a dynamic mesh, whereas the chordae tendineae are represented using a sub-grid model based on the "Actuator Line Method" (ALM) of [32]. This method is commonly used for simulating rotating wind turbines.

The purpose of this paper is twofold. First, to analyze and discuss to what extent the chordae tendineae are relevant for the flow conditions, or whether the direct effect on flow can be neglected. Second, to discuss whether it is necessary to include the chordae tendineae in practical CFD simulations or not.

The outline of the paper is as follows: We first describe a CFD model of the left ventricle during systole and a sub-grid model for the effect of the chordae tendineae on the fluid flow. To simulate the resistance of the chordae tendineae to fluid flow, we model them as cylinders in cross flow. We validate the subgrid model against a rigorous simulation of a transient test case. Finally, we present simulation results of a heart during systole and discuss the effect of the chordae tendineae on systolic flow.

2. Method

2.1. CFD model of the left ventricle

We use an existing model for the left ventricle (LV) during systole [3]. The model has prescribed LV wall movement and is based on segmented 3D echocardiography recordings of a healthy female volunteer as described in the following.

2.1.1. 3D echocardiography and segmentation of the LV

In a previous work [3], the left ventricle volume of a 30 years old female volunteer was acquired by real-time three-dimensional echocardiography (RT3DE) (also known as four-dimensional echocardiography). The volume was acquired during apnea over 4 heart cycles. The segmentation of the endocardial LV wall resulted in 27 closed three dimensional surface meshes, one for each time frame. Fig. 1 shows the surface mesh at one instance during the cardiac cycle. Each mesh consists of 1946 nodes and 3888 triangular cells, and were used to create the prescribed subject-specific LV movement throughout systole. The mesh was further refined for better accuracy in the CFD simulations, as described in Ref. [33].

The segmented LV wall from the 3D echocardiography (Fig. 1) does not include the mitral valve or the aorta. The physiological MV and the proximal part of the ascending aorta (AAo) have therefore been reconstructed from the same RT3DE recordings as for the LV wall and included into the original segmented LV surface mesh. The details can be found in Ref. [3].

The MV geometry was reconstructed from its physiological shape at peak systole and set to be static throughout the simulation. The subject-specific 3D MV model is shown in Fig. 2.

The ascending aorta is the first section of the aorta, commencing at the upper part of the LV base. The shape and tilting angle of the AAo was traced in the recordings and attached to the LV. During the simulation the AAo will deform in accordance to the LV base. The aortic root with its sinuses of Valsalva, which is the first part of the AAo, was simplified to a tube. The length of the AAo was set to minimize the influence of the outflow conditions on the flow field of interest. Fig. 3 shows the complete subject-specific model at different instances during systole.

2.1.2. Implementing the dynamic mesh in CFD

The time step in the CFD-simulation (0.0005 s) is significantly smaller than the time step between the recorded frames. This required

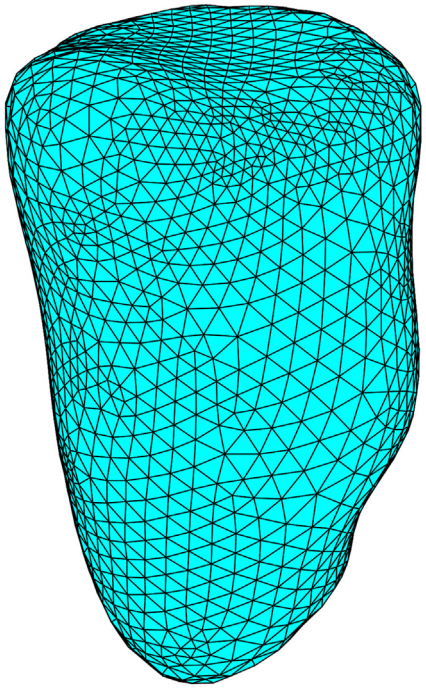

Fig. 1. Closed three dimensional surface mesh of the endocardial LV wall at one instance of the cardiac cycle.

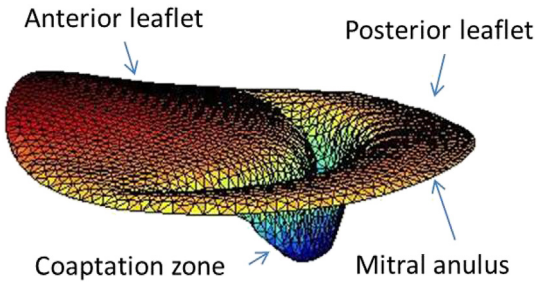

Fig. 2. 3D model of the physiological mitral valve at peak systole. As seen in the figure, the curvature of the normal, healthy mitral leaflets is approximately flat at peak systole.

new intermediate meshes for each CFD time step to be calculated between the segmented time frames. The meshes were generated by cubic spline interpolation of the mesh node coordinates in time. The spline polynomials were precomputed in the form of a coefficient table, using the standard spline routine in Matlab.

The simulation period is the systolic part of the heart cycle from the onset of aortic valve (AoV) opening to AoV closure in end-systole, i.e. the isovolumetric contraction in start-systole is not included. The length of this period was, in our recordings, measured to 285 ms in a heart cycle of 962 ms [3]. The start geometry is from the segmented LV wall at AoV opening.

The prescribed LV wall movement was implemented as a User-Defined-Function (UDF) and used as a boundary condition in our CFD simulations. The AAo was set to deform in accordance to the LV, whereas the MV was set to be static throughout the simulation.

2.2. CFD closure model for the chordae tendineae

A sub-grid model was used to represent the chordae tendineae. When the blood flows across the chordae tendineae there will be a drag force. For practical purposes the force can be calculated by considering the chordae as cylinders, for which correlations for the drag force are well known from the literature. In the following the theory of fluid drag

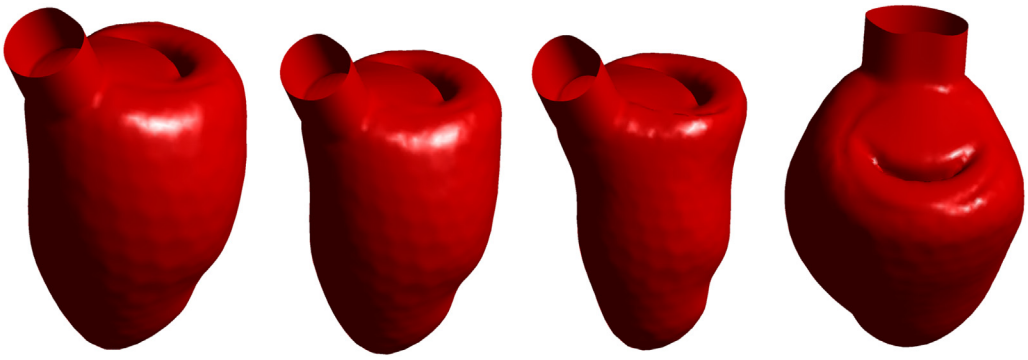

(a) start systole (b) peak systole (c) end systole (d) mitral smiley

Fig. 3. The complete subject-specific 3D model of the LV including the MV and the proximal part of the AAo. The AAo is longer in our model, but cut only the first part is shown here Figure (a) is from start systole, (b) is from peak systole, i.e. 100 ms into the simulation from AoV opening and (c) is from end systole. Figure (d) shows the model from an atrial view, where the mitral "smiley" is clearly visible.

on cylinders is developed.

2.2.1. Flow across cylinders

Consider the drag force from the blood on a chordae, considering the chordae as an approximate cylinder. For moderate Reynolds numbers (below the drag crisis), Re, one can basically assume that the drag force is orthogonal to the cylinder and due to the velocity component, $V_\perp$, in the orthogonal direction ("Cross-flow principle", [34]). The velocity decomposition is shown in Fig. 4.

The drag force per length of cylinder, $\boldsymbol{D}$ $[N/m]$, can be approximated by the Morison equation, Equation (1):

$$\mathbf{D} = \overbrace{C_M \rho \frac{\pi d^2}{4} \frac{\partial \boldsymbol{V}_\perp^\infty}{\partial t}}^{I} + \overbrace{C_d d \frac{1}{2} \rho \|\boldsymbol{V}_\perp^\infty\| \boldsymbol{V}_\perp^\infty}^{II} \tag{1}$$

where t is time, d is the cylinder diameter, ρ is the fluid density, $\boldsymbol{V}_\perp^\infty = \boldsymbol{V}^\infty - (\boldsymbol{\tau} \cdot \boldsymbol{V}^\infty)\boldsymbol{\tau}$ is the free-stream velocity component normal to the cylinder, $\boldsymbol{V}^\infty$ is the free-stream velocity and $\boldsymbol{\tau}$ is a unit vector tangential to the cylinder (axial direction).

The first term (I) on the right hand side is due to the acceleration of the fluid around the cylinder (added mass effect) plus the force from the pressure gradient that produces the fluid acceleration (Krylov force). The inertia coefficient for a cylinder is $C_M = 2$.

The second term (II) is the steady state drag, where $C_d(Re)$ is the drag coefficient and $Re = \frac{\rho \boldsymbol{V}_\perp^\infty d}{\mu}$ is the Reynolds number. We use a simple approximate correlation (~20% relative error) for the drag coefficient in the range $0.1 < Re < 250000$ as given by Ref. [35]:

$$C_d = 1 + \frac{10}{Re^{\frac{2}{3}}} \tag{2}$$

A more accurate relation (< 8% relative error) valid for $1 \times 10^{-4} < Re < 2 \times 10^5$ is given by Ref. [36]:

$$C_d = 1.18 + \frac{6.8}{Re^{0.89}} + \frac{1.96}{Re^{0.5}} - \frac{0.0004Re}{1 + 3.6 \times 10^{-7} Re^2} \tag{3}$$

We argue in Appendix A that the transient term is negligible compared to the second term when applied to the drag on chords. Thus,

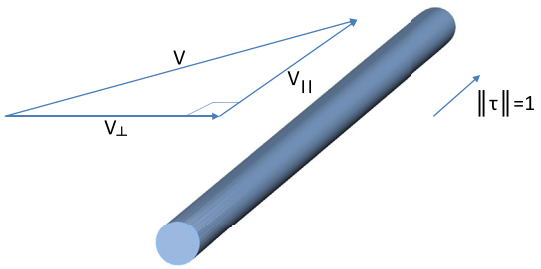

Fig. 4. Flow across cylinder.

Equation (1) reduces to:

$$\mathbf{D} \approx C_d d \frac{1}{2} \rho \|\boldsymbol{V}_\perp^\infty\| \boldsymbol{V}_\perp^\infty \tag{4}$$

2.2.2. Implementation as source terms in CFD codes

The drag force from the fluid on the chordae, $\boldsymbol{D}$, is described by Equation (4), and is a force per meter chordae. By Newtons third law there is a reaction force from the chordae on the fluid. However, as we do not resolve the detailed chordae geometry on the computational mesh we need to approximate the reaction force as a source term.

To achieve this we use the Actuator-Line Method by Ref. [32]. The basic idea is to distribute the drag force over a region of the order of radius ε [m] from the force. Ideally, ε should be small. However, it can not be smaller than about two times the local mesh size for stability reasons. Also, the drag formulae (Equation (2) or 3) are based on the freestream velocity, i.e. the local fluid velocity that is unperturbed by the presence of the chordae, which means that ε should not be too small. Thus, there is a trade-off. In the present simulations we have used $\varepsilon \sim 0.005m$.

The source term is calculated as follows:

1. The chordae are divided into short elements of length dx_i, $i = 1,2, ...N$.
2. The drag force of element i is $\boldsymbol{D_i} \equiv \boldsymbol{D}(\boldsymbol{x_i})dx_i$ where $\boldsymbol{x_i}$ is the centre of the element.
3. The discrete $\boldsymbol{D_i}$ is distributed in space using a distribution function $\eta(\boldsymbol{r})$.

The distribution function used is given by Equation (5) [32]:

$$\eta(\boldsymbol{r}) = \frac{1}{\varepsilon^3 \pi^{3/2}} \exp\left[-\left(\frac{|\boldsymbol{r}|}{\varepsilon} \right)^2 \right] \tag{5}$$

Mathematically, the volume integral of the distribution function over all space integrates to one. However, close to walls one needs to normalize to account for what falls outside the fluid domain:

$$\tilde{\eta}(\boldsymbol{r}) = \frac{\eta(\boldsymbol{r})}{\iiint_{\mathbf{fluid}} \eta(\boldsymbol{r}) dV} \tag{6}$$

Summing over all drag elements, the momentum source term $[N/m^3]$ becomes:

$$\boldsymbol{f}(\boldsymbol{x}) = \sum_i \boldsymbol{D}_i \cdot \tilde{\eta}(\boldsymbol{x} - \boldsymbol{x}_i) \tag{7}$$

The source term was implemented as a user-defined-function (UDF) in ANSYS Fluent [37].

2.3. Ventricular pressure drop due to the chordae tendineae

We derive a relation for the contribution to pressure drop in the ventricle that is caused by the drag across the chordae. As pressure drop

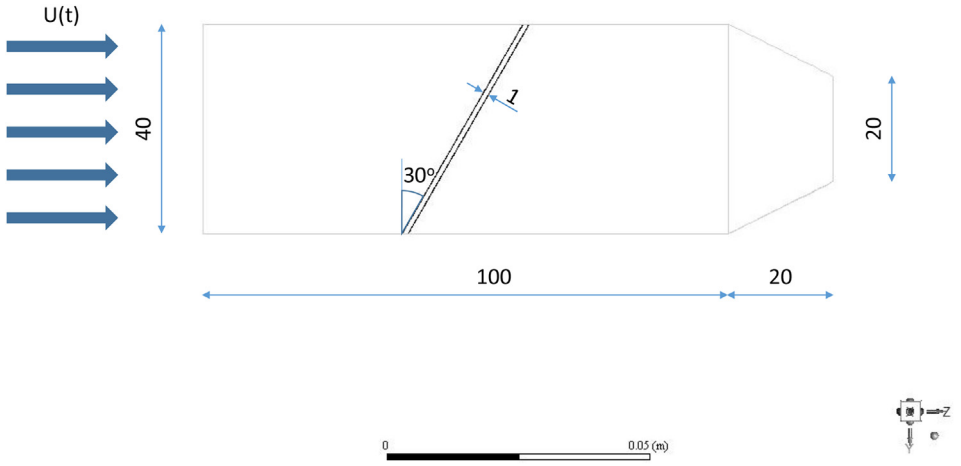

Fig. 5. Single Chordae in accelerated flow.

times flow rate equals the power loss, we can compute the contribution to pressure drop as power loss per flow rate. The instantaneous power loss per length of chordae, w $[W/m]$, can be expressed as:

$$w = |\boldsymbol{D} \bullet \boldsymbol{V}^{\infty}| \tag{8}$$

The loss is dissipated into heat. The equivalent pressure drop, $\Delta p_{chordae}$ $[Pa]$, relative to the aortic outflow, Q $[m^3/s]$, can thus be found by integrating the power loss over the chordae length, s $[m]$, and dividing by the outlet flow rate:

$$\Delta p_{chordae} = \frac{1}{Q} \int_{chordae} |\boldsymbol{D} \bullet \boldsymbol{V}^{\infty}| ds \tag{9}$$

2.4. Validation of the actuator line method

In order to validate the ALM approach and implementation, we have simulated a simple test case with ALM and compared against a rigorous simulation where the details are resolved. The test case is shown in Fig. 5 and consists of a single 1 mm cylinder placed at a 30° angle in a 40 mm × 40 mm channel. The channel walls are taken as frictionless. The transient inlet velocity as function of time is shown in Fig. 6 and resembles the velocity across chordae during systole. Peak systole is at approximately t = 0.1 s. Physical properties are as for blood ($\mu = 3.5$ cP, $\rho = 1050$ kg/m^3).

For the rigorous simulation we have used the mesh shown in Fig. 7, which is refined in the vicinity of the cylinder to ensure proper flow resolution. A grid sensitivity test was performed to ensure proper spatial resolution. This was done by comparing the flow calculated with 1.44×10^6 and with 4.0×10^6 grid cells. As there was no significant difference, the grid with 1.44×10^6 cells was used.

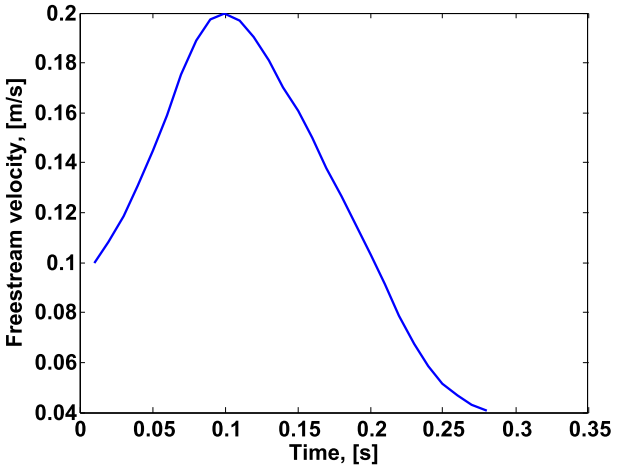

Fig. 6. Freestream velocity, U(t), as function of time.

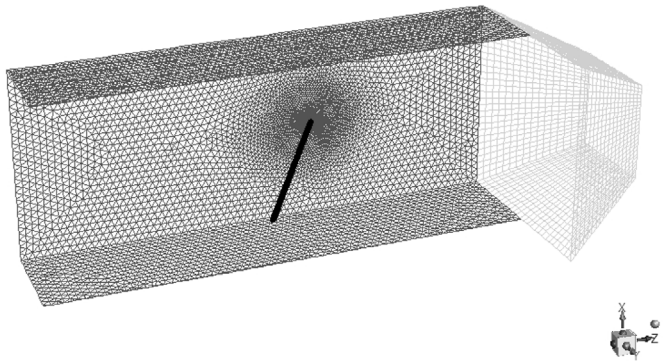

Fig. 7. Mesh for rigorous simulation. Showing only one side of the channel wall.

Fig. 8 shows the velocity magnitude around the cylinder at the xz symmetry plane at peak systole. The Reynolds number based on crossflow velocity is about 50, which according to theory is just on the border of onset of vortex shedding. In the simulations there is no sign of vortex shedding at this point.

For the simplified ALM simulations a uniform hex-mesh was used (Fig. 9).

Fig. 10 shows the calculated force per unit length of cylinder at peak systole (U = 0.2 m/s). The drag force in the ALM method is orthogonal to the cylinder as intended.

Fig. 11 compares the net force on the cylinder calculated by different methods. The ”analytical:total” is the prediction by using equation (1) directly based on the specified inlet velocity. This is composed of a drag term and inertia term shown as dotted lines, and it can be seen that the inertia term is an order of magnitude smaller than the drag term. The ALM method as currently implemented ignores inertia, and only predicts the viscous drag term. As can be seen, the FLUENT ALM prediction is close to the ”Analytical:Drag” as intended.

The peak of the rigorous FLUENT simulation comes about 5 ms before the Analytical result. The lead increases to about 15 ms after peak systole. This indicates that the balance between the inertia term and the viscous drag term in the Morison equation is not completely accurate. Also, the Morison equation ignores history effects. Nevertheless, the small time lag in the Morison equation compared to the rigorous simulation is unlikely to have much practical significance.

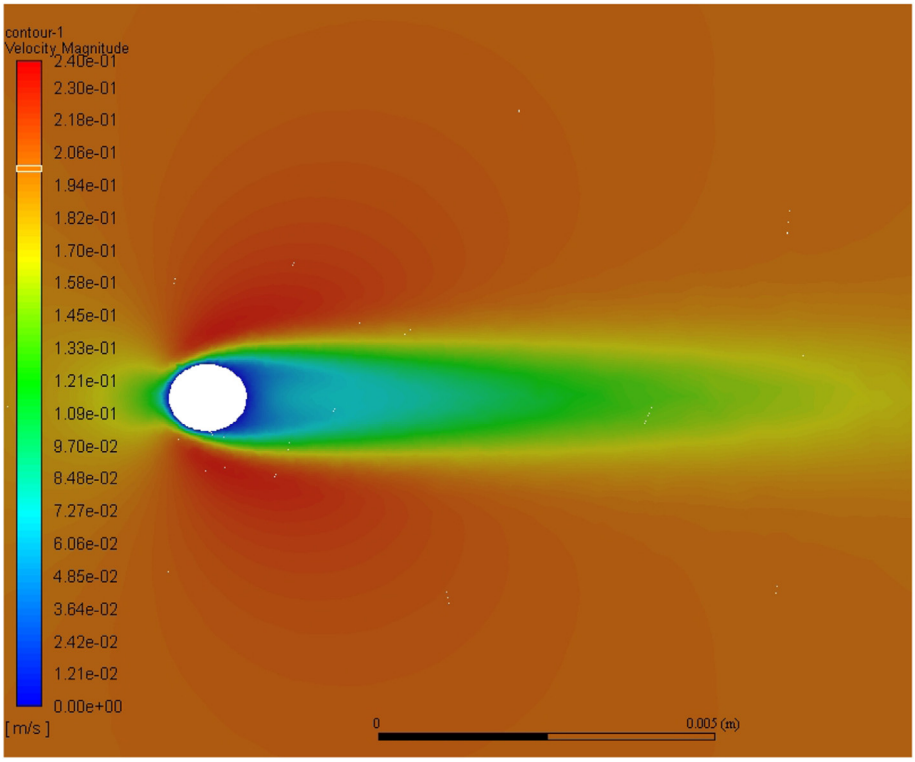

Fig. 8. Velocity field at symmetry plane (xz-plane) for rigorous simulation, peak systole (velocity U = 0.2 m/s).

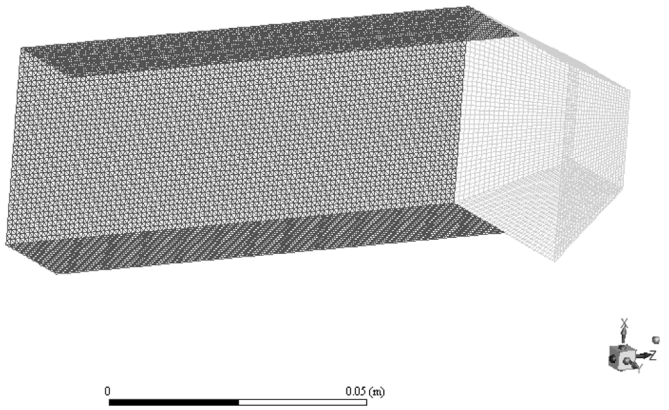

Fig. 9. Mesh for ALM simulation. Mesh size 1.5 mm. Showing only one side of the channel wall.

2.5. Construction of the chordae tendineae geometry

The geometry of the chordae tendineae in general is well described in the literature. For example Lam et al. [38], investigated the chordae tendineae of 50 human hearts. They found that an average of 25 chordae insert into the mitral valve. Of these, nine pass to the anterior leaflet (seven rough zone chordae and two strut chordae), 14 to the posterior leaflet (10 rough zone chordae, two cleft chordae and two basal chordae) and two are inserted into the commissures.

We do not have an actual patient-specific geometry of the chordae tendineae for the simulated case. For the present numerical demonstration we model the chordae tendineae very simplistically, as shown in Fig. 12. This geometry was constructed manually by using the computer mouse to pick the insertion points of the chordae into the mitral valve, snapped to the nearest node of the surface mesh. In our model there are 6 chordae originating from each papillary muscle, each chordae then split up into three branches before a total of 36 chords are inserted near the free edge of the mitral valve. As a modeling simplification, the chordae originate from the same point at their respective papillary muscle. Fig. 12 c) shows a close-up of the distribution of the chordae tendineae in our model.

For the purpose of the demonstration we set the chordae diameter uniformly as 1 mm.

2.6. Solver settings and fluid properties

The system was solved in FLUENT using first order implicit time integration (PISO) with a fixed time step of 0.0005 s, second order spatial discretization for pressure and second order upwind discretization for momentum. Blood properties were: density 1050 kg/m^3, viscosity 3.5 cP.

3. Results

3.1. Velocity field and resulting forces on the chordae

Simulation results are presented for the time until peak systole (t = 100 ms), which is when the forces are largest. After peak systole, the velocities and forces decrease again. Fig. 13 shows the magnitude of the flow velocity at the central cross section of the ventricle (long-axis view) at four different instances (i.e. t = 10, 20, 50 and 100 ms). The overall flow is from the apex towards the aorta. As a comparison, the same simulation runs without including the chordae tendineae are shown in Fig. 14. The overall flow patterns with and without the chordae tendineae are almost indistinguishable. This is demonstrated in Fig. 15, showing the difference in velocity magnitude with and without chordae at t = 100 ms. As can be seen the maximum velocity difference in the simulations is only 0.045 m/s, in a small area in the aorta. In most of the domain the velocity difference is less than 0.02 m/s.

Fig. 16 shows the calculated flow velocity at the chordae position. As can be seen, the velocity is increasing until peak systole. The highest velocities at the chordae occur near the mitral valve where the flow pass the coaptation zone.

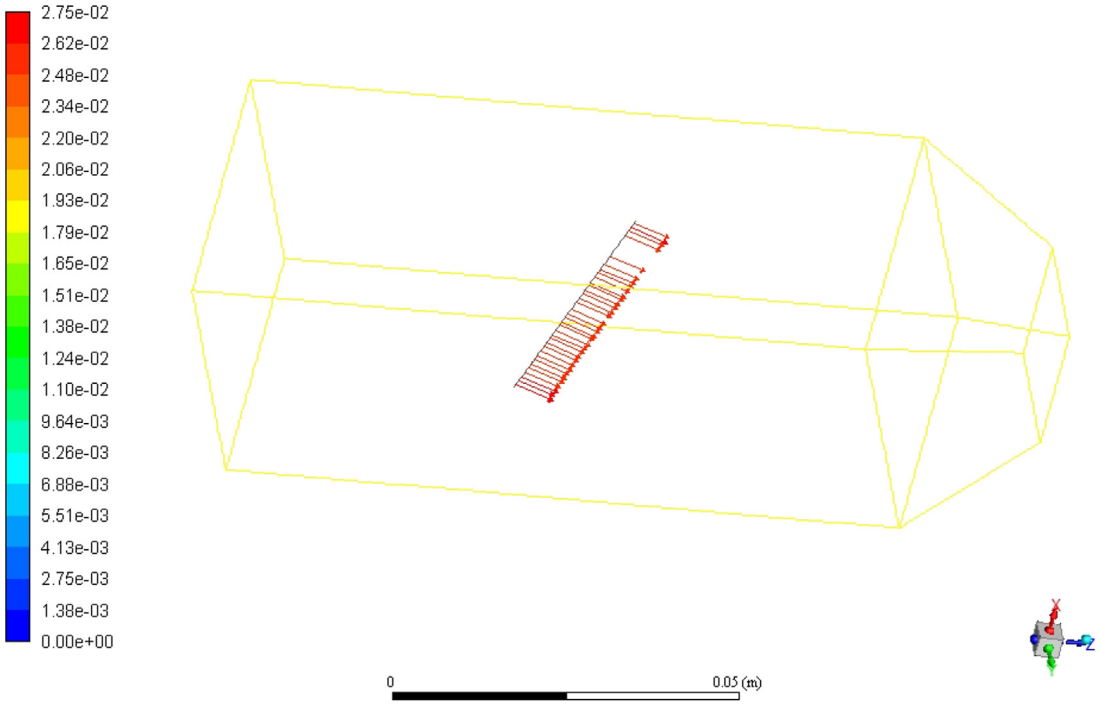

Fig. 10. Force per chord length calculated by ALM, [N/m]. Peak systole (velocity U = 0.2 m/s).

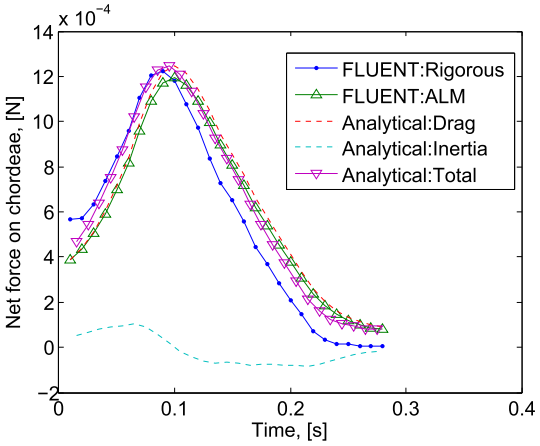

Fig. 11. Net force on cylinder as function of time, calculated by various methods, [N/m].

The fluid drag forces per length of the chordae tendineae are shown in Fig. 17. The fluid drag forces are quite small, of the order of 10–30 mN per meter chordae. They are largest close to the coaptation zone where the fluid velocity is highest. Closer to the tip of the papillary muscles the forces are smaller due to lower fluid velocities.

Table 1 shows the equivalent pressure drop caused by the chordea as calculated by Equation (9). As can be seen, the pressure drop at peak systole ($t = 100ms$) is only 2.7 Pa, or about 0.02 $mmHg$. This is negligible compared to the $\sim$ 100 $mmHg$ pressure difference of the heart.

4. Discussion

4.1. Pressure drop and pumping work in systole

During systole the heart has to provide work in order to pump blood against the aortic pressure. This is the useful work of the heart, and any work that is much smaller than this is insignificant in comparison. For the ventricle in this study (Section 2.1), a volume of about $V = 56ml$ blood is pumped against an aortic pressure difference of about $\Delta p \sim 100mmHg$, which means that a useful work of $W = V\Delta p \sim 0.75J = 1.8 \times 10^{-4}kcal$ has to be provided per heart beat. This provides a reference for comparing the pressure drop and work losses due to fluid dynamic drag across the chordae tendineae.

4.1.1. Influence of the chordae tendineae on pressure drop and flow

That the pressure drop penalty of the chordae tendineae in a healthy heart only correspond to about 2.7 Pa (= $0.02mmHg$) at the maximum should not come as a complete surprise from an evolutionary perspective, as other solutions would be favored if otherwise. The heart needs to pump blood against more than a 100 mmHg pressure difference; thus the power loss due to chordae is negligible in comparison. One can obtain an order-of-magnitude estimate of the forces on the chordae by assuming a velocity of the order of $V = 0.15m/s$ across the chordae (typical value from the simulation shown in Fig. 16). The drag coefficient according to Equation (4) is then $Cd \approx 2$. Thus the drag is about $D \sim C_d d \frac{1}{2}\rho V^2 = 0.02N/m$ which is comparable to the number obtained by CFD.

4.2. Vortex formation behind the chords

By treating the chordae tendineae using source terms the tiny details of the flow around the chordae are not resolved. To do so, one would have to resolve the geometry of the chordae individually using an excessively fine grid, which is unpractical.[1] However, the details are known from theory.

For Reynolds numbers larger than about 47 ($Re_d = \frac{\rho V_\perp^\infty d}{\mu}$), vortices will form behind a chordae in crossflow[2] (von Kármán vortex street). This manifests itself as a slight vibration of the chordae. For a 1 mm chordae in blood, this corresponds to a velocity larger than about[3] $V_\perp^\infty \approx 0.15\ m/s$. The frequency of the vortex shedding for cylinders is

[1] Some papers in the literature actually resolve the chordae, e.g. Ref. [31]. However, the aim of the present work is towards model simplification.

[2] Assuming they can be approximated as cylinders.

[3] Assuming blood viscosity $\mu = 3.5 \times 10^{-3}kg/ms$ and density.$\rho = 1050kg/m^3$

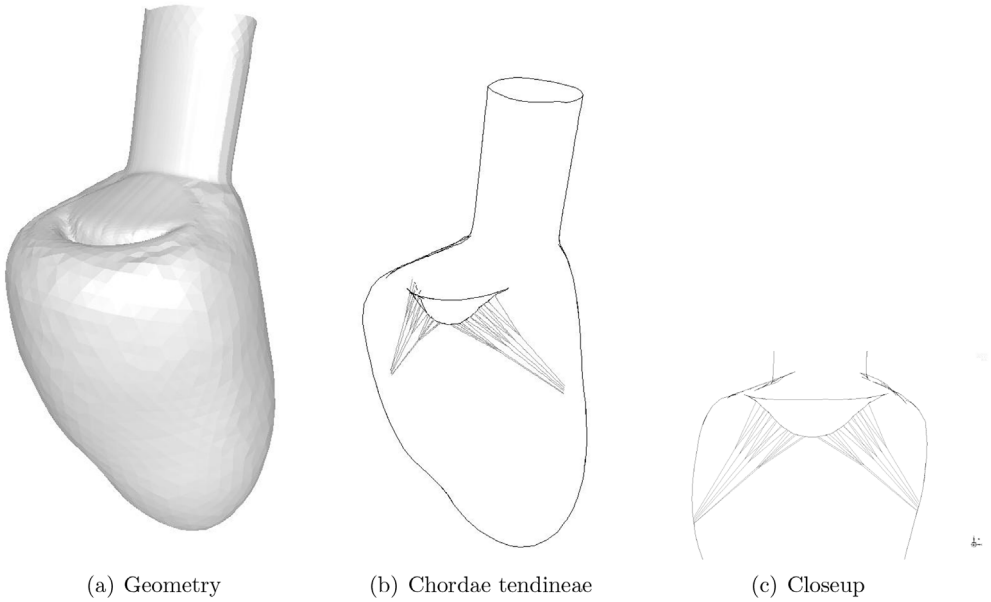

Fig. 12. Simplistic chordae tendineae geometry.

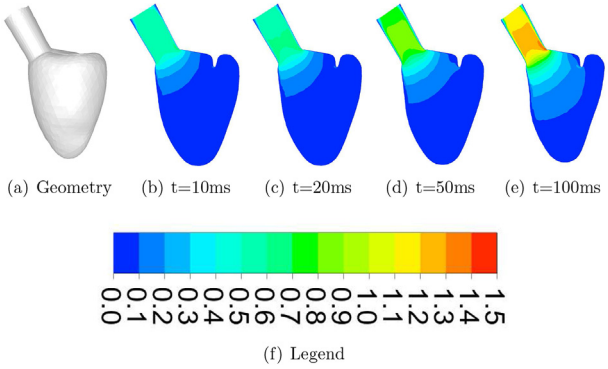

Fig. 13. Velocity magnitude, [m/s], at the central cross section (with chordae). Peak Systole at 100 ms

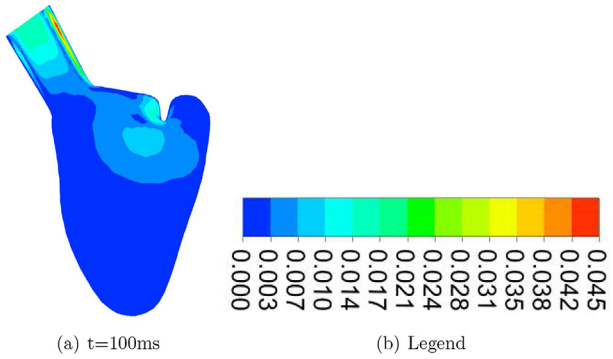

Fig. 15. Difference in velocity magnitude, [m/s], at the central cross section with and without chordae. Peak Systole at 100 ms

given by the Strouhal number, $Str = \frac{fd}{V_{\perp}^{\infty}} \approx 0.2$, where f $[Hz]$ is the vortex shedding frequency. At $V_{\perp}^{\infty} \approx 0.15$ m/s the shedding frequency for a 1 mm chord is thus $f \approx 30$ Hz. The vortices dissipate into heat downstream of the chordae. As the overall pressure drop caused by the chordae is very small one may hypothesize that these vortices have only minor effects on the heart function.

4.3. Effect of inertia on the drag on the chordae tendineae

As explained in section 2.2.1 the drag forces on the chordae tendineae are in principle the sum of a steady state drag and inertia forces due to fluid acceleration. In Appendix A it is shown that the inertia forces on the chordae are much smaller than the steady state drag. From the discussion above the steady state drag on the chordae is again small compared to the pumping forces of the heart.

4.4. Relation to complementary work

In this study, the focus has been on the influence of the chordae tendineae, thus the papillary muscles and the trabecula have not been modeled. However, there has been recent work on the trabeculae and

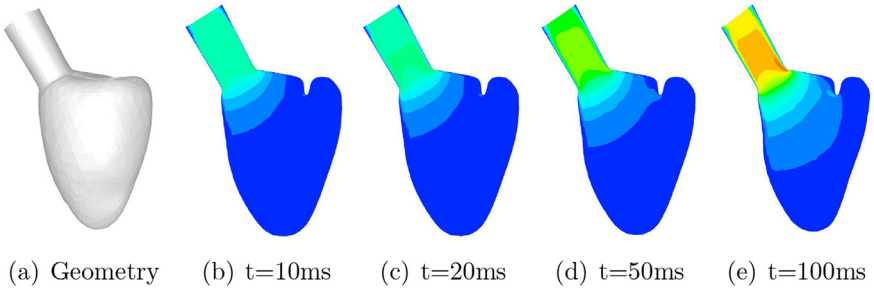

Fig. 14. Reference simulation without chordae tendineae. Velocity magnitude, [m/s], at the central cross section. Peak Systole at 100 ms. Legend is the same as in Fig. 13.

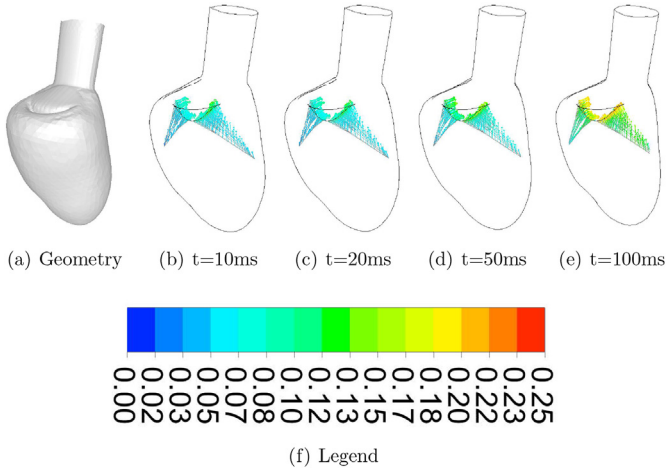

Fig. 16. Velocity at chordae position, [m/s], as function of time. Peak Systole at 100 ms

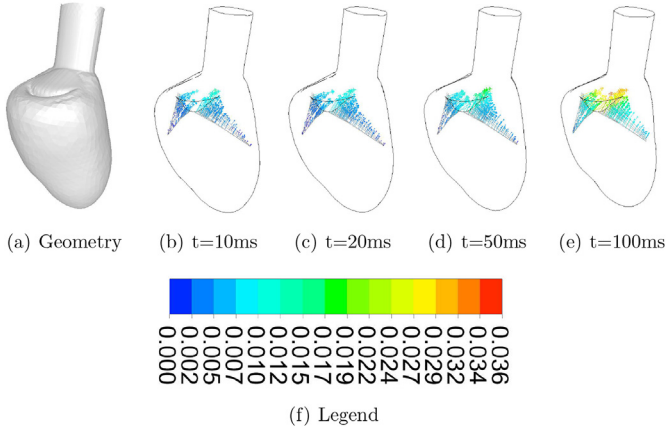

Fig. 17. Drag force per length of chordae, [N/m], as function of time. Peak Systole at 100 ms

Table 1
Equivalent pressure drop caused by the chordae tendineae as function of time.

Time, [ms]	Pressure drop, [Pa]
10	0.7
20	0.7
50	1.1
100	2.7

papillary muscles in the literature, both in the left ventricle [19–24] and in the right ventricle [25]. Gao et al. [19] discusses the morphology of the papillary muscles and trabeculae and describes a method of geometry reconstruction from high resolution CT. They show how to represent the structures accurately by means of curve skeletons. Sacco et al. [23] and Sacco et al. [25] studied the effect of the trabeculae and papillary muscles on haemodynamics and pressure drop in the left and right ventricle, respectively. In these works, the endocardial structures are modeled in detail and the flow is simulated in a simplified (static) heart model. Kulp et al. [20] performed patient-specific simulations of blood flow in the left ventricle based on high-resolution CT imaging and an immersed boundary method. By flow field visualization they show the interaction between the blood and the trabeculae in high detail, and compared the flow fields between a healthy heart and two diseased hearts Lantz et al. [22]. developed a framework for computing patient specific hemodynamics based on time-resolved CT-images, which was applied to a patient with a dilated left ventricle. The model included papillary muscle motion and the folding and unfolding of left ventricular trabeculae, and the results indicated that these are important aspects to consider when computing cardiac blood flow. They indicated that these features strongly interacted with the blood, which could not be observed in a simplified model Vedula et al. [24]. investigated the impact of trabeculae and papillary muscles on the hemodynamics of the left ventricle, using a high resolution immersed boundary method. Two different models were compared, the most detailed one comprising a trabeculated endocardium including trabeculae and papillary muscles. Conclusions are that although the trabeculae and papillary muscles significantly increase the viscous dissipation in the flow, the magnitude of this increase is negligible compared to the total pressure work associated with the left ventricle. However, the papillary muscles act in concert to guide the mitral jet deeper into the apical region and energize the apical flow. Another significant effect of the papillary muscles on the flow pattern is the migration of the mitral jet from the posterior wall towards the anterior wall of the LV; however, it was unclear whether patient-specific variations in the morphology of the papillary muscles would modulate this effect. These papers can be seen as complementary to the present work, which has focus on the chordae tendineae.

Also, there has been recent work on the modeling of the chordae tendineae [26–28]. Meschini et al. [27] modeled Fluid-Structure-Interaction of a mitral valve with chordae, using a simplified (static) heart model and a simplified model of the chordae where the chords are lumped into four main bundles. Compared to the present work the bundling appear to yield some overprediction of the drag on the chordae (overprediction of energy dissipation due to the chordae); otherwise the approach for representing the chordae is very simple and interesting as a direction for practical/simplified models if more attention is given to get better prediction of chordae drag. Other recent work is Caballero et al. [26]; who calculate fluid flow in a mitral valve and chordae load distributions using Smoothed Particle Hydrodynamics to simulate the flow. They also quantify the amount of regurgitation. The article has focus on load distributions and rupture of chordae and not so much on the effects of the chordae on the flow Singh-Gryzbon et al. [28]. developed a computational model of the flow in a tricuspid valve (TV), based on high resolution μCT of a porcine TV. The flow in the valve was modeled as well as studied experimentally in a cylindrical test chamber with valve. Also this paper has focus on the structure part and stresses in the chordae; and thus is complementary to the present paper.

4.5. Limitations of the study

By representing the chordae tendineae by means of source terms, the main effects of the chordae on flow and pressure drop are captured. What is not resolved in the CFD simulations are the tiny flow structures around the chordae. These structures are known from literature (von Kármán vortex street). As the drag force on the chordae is relatively weak one may hypothesize that these structures have only minor effects on the heart function.

The CFD simulations have only been performed for the systole. However, the order-of-magnitude estimates of the effects of the chordae tendineae also apply for the diastole. Thus, the effects of the chordae on the overall flow pattern during diastole are also expected to be minor, however, this must be studied in order to conclude.

5. Conclusion

The effect of the chordae tendineae on blood flow during ventricular systole has been analyzed by CFD. Within this model the chordae tendineae were represented using a sub-grid model based on the ”Actuator Line Method”. By this combination we resolve the main features of the flow on a dynamic mesh while avoiding the complexities of tiny details

around the chordae tendineae.

The fluid forces on the chordae tendineae can be considered to be the combination of inertia forces (added mass + Krylov) and a steady state drag. An order-of-magnitude analysis shows that the steady state drag dominates compared to the inertia forces, and the inertia effects can be neglected in comparison. From a fluid pressure drop point of view, also the steady state drag has an insignificant effect in a healthy heart. Thus, the chordae tendineae do not result in any work inefficiencies (power loss) in the healthy heart.

At velocities above approximately $0.15 m/s$, which may occur close to peak systole, there can be vortex shedding behind the chordae (von Kármán vortex street). This manifests itself as a weak vibration of the chordae at a frequency of around $30 Hz$. As the fluid drag forces are quite weak it is unlikely that this has any clinical implications (in a healthy heart).

Thus, it seems that for simulating ventricular fluid flow and pressure drop during systole in the healthy heart one can follow the current practice and ignore the chordae tendineae. However, there can be local effects such as small vortices behind the chordae. Whether such effects are important for a particular application must be evaluated for the given case.

Author's contributions

All authors read and approved the final manuscript.

Conflicts of interest

The authors have no conflict of interests (Competing interests: None declared, Funding: None, Ethical approval: Not required).

Statements of Human and animals studies

No human or animal studies were carried out by the authors for this article.

Acknowledgements

This study was financed internally by SINTEF Materials and Chemistry.

Nomenclature

Latin symbols

C_d	Drag coefficient, $[-]$
C_M	Inertia coefficient, $[-]$
D	Drag per chordae length, $[N/m]$
d	Chordae diameter, $[m]$
D_i	Drag on small chordae element, $[N]$
$f(x)$	Momentum source term, $[N/m^3]$
Δp	Pressure drop, $[Pa]$
Q	Flow rate, $[m^3/s\ ]$
r	Distance from force centre, $[m]$
Re	Reynolds number of Chordae, $[-]$
s	Length along chordae, $[m]$
t	Time, $[s]$
V	Fluid velocity, $[m/s\ ]$, or volume, $[m^3]$
$V_{\perp}^{\infty}$	Velocity component parallel to chordae, $[-]$
$V_{\parallel}^{\infty}$	Velocity component orthogonal to chordae, [..]
w	Power loss per chordae length, $[W/m]$
x	Position vector, $[m]$

Greek symbols

ε	Length scale for η, $[m]$
η	Source distribution function, $[m^{-3}\ ]$
ρ	Fluid density, $[kg/m^3\ ]$
τ_{chord}	Chordae flow time scale, $[s]$
τ_{global}	Global time scale, $[s]$
$\tilde{\eta}$	Normalized source distribution function, $[m^{-3}]$

Superscripts

∞	Freestream value away from chordae

Subscripts

⊥	Component orthogonal to chordae
‖	Component parallel to chordae
i	Small element #i on chordae

Appendix A. Order of magnitude analysis of drag terms

We perform an order-of-magnitude analysis to demonstrate that the transient drag term in Equation (1) can be ignored. The time derivative is of the order $\frac{\partial V_{\perp}^{\infty}}{\partial t} \sim \frac{V}{\tau_{global}}$ where V is a typical velocity during systole ($\sim$ 1 m/s in the aorta and $\sim$ 0.1 m/s below the coaptation zone) and τ_{global} is a global time scale of the order of the time to peak systole ($\sim$ 0.1 s). Ignoring constants of the order of one, we get the order of magnitude:

$$C_M \rho \frac{\pi d^2}{4} \frac{\partial \boldsymbol{V}_\perp^\infty}{\partial t} \sim \rho d^2 \frac{V}{\tau_{global}} \tag{A.1}$$

The second term is larger than[4] or of the order:

$$C_d d \frac{1}{2} \rho \| \boldsymbol{V}_\perp^\infty \| \boldsymbol{V}_\perp^\infty \gtrsim d \rho V^2 \tag{A.2}$$

Introducing the time scale for the fluid to flow past the chordae, $\tau_{chord} \equiv \frac{d}{V}$, the ratio between the two terms becomes:

$$\frac{C_M \rho \frac{\pi d^2}{4} \frac{\partial \boldsymbol{V}_\perp^\infty}{\partial t}}{C_d d \frac{1}{2} \rho \| \boldsymbol{V}_\perp^\infty \| \boldsymbol{V}_\perp^\infty} \lesssim \frac{\rho d^2 \frac{V}{\tau_{global}}}{d \rho V^2} = \frac{d/V}{\tau_{global}} = \frac{\tau_{chord}}{\tau_{global}} << 1 \tag{A.3}$$

Thus, as long as the time scale for a fluid particle to pass the chordae is much smaller than the overall time scale of the systole the transient term can be safely ignored. For example, for a cross-flow velocity of the order of 0.1 m/s across a 1 mm chordae the chordae time scale is (0.001 m)/(0.1 m/s) = 0.01 s = 10 ms. The time to peak systole is approximately 100 ms; thus the ratio of the terms becomes (10 ms)/(100 ms) = 0.1. That is, the inertia term is expected to be about one order of magnitude smaller than the viscous drag term.

References

[1] V. Prot, Modelling and Numerical Analysis of the Porcine and Human Mitral Apparatus, Ph.D. thesis. Ph. D. Thesis Department of Structural Engineering, NTNU, Norway, 2008.

[2] A.M. Bavo, A.M. Pouch, J. D, J. Vierendeels, J.H. Gorman, R.C. Gorman, P. Segers, Patient-specific cfd simulation of intraventricular haemodynamics based on 3d ultrasound imaging, Biomed. Eng. Online 15 (2016).

[3] S.K. Dahl, Numerical Simulations of Blood Flow in the Left Side of the Heart, Ph.D. thesis Norwegian University of Science and Technology, 2012.

[4] A. Dimasi, E. Cattarinuzzi, M. Stevanella, C.A. Conti, E. Votta, F. Maffessanti, N.B.J. Ingels, A. Redaelli, Influence of mitral valve anterior leaflet in vivo shape on left ventricular ejection, Cardiovascular Engineering and Technology 3 (2012) 388–401.

[5] T. Doenst, K. Spiegel, M. Reik, M. Markl, J. Hennig, S. Nitzsche, F. Beyersdorf, H. Oertel, Fluid-dynamic modeling of the human left ventricle: methodology and application to surgical ventricular reconstruction, Ann. Thorac. Surg. 87 (2009) 1187–1195.

[6] F. Domenichini, G. Pedrizzetti, Intraventricular vortex flow changes in the infarcted left ventricle: numerical results in an idealised 3d shape, Comput. Methods Biomech. Biomed. Eng. 14 (2011) 91–101.

[7] F. Domenichini, G. Querzoli, A. Cenedese, G. Pedrizzetti, Combined experimental and numerical analysis of the flow structure into the left ventricle, J. Biomech. 40 (2007) 1988–1994.

[8] S.N. Doost, L. Zhong, B. Su, Y.S. Morsi, The numerical analysis of non-Newtonian blood flow in human patient-specific left ventricle, Comput. Methods Progr. Biomed. 127 (2016) 232–247.

[9] A. Imanparast, N. Fatouraee, F. Sharif, The impact of valve simplifications on left ventricular hemodynamics in a three dimensional simulation based on in vivo mri data, J. Biomech. 49 (2016) 1482–1489.

[10] S.S. Khalafvand, L. Zhong, E.Y.K. Ng, Three-dimensional cfd/mri modeling reveals that ventricular surgical restoration improves ventricular function by modifying intraventricular blood flow, International Journal for Numerical Methods in Biomedical Engineering 30 (2014) 1044–1056.

[11] S. Krittian, T. Schenkel, U. Janoske, H. Oertel, Partitioned fluid-solid coupling for cardiovascular blood flow: validation study of pressure-driven fluid-domain deformation, Ann. Biomed. Eng. 38 (2010) 2676–2689.

[12] T.B. Le, F. Sotiropoulos, Fluid structure interaction of an aortic heart valve prosthesis driven by an animated anatomic left ventricle, J. Comput. Phys. 244 (2013) 41–62.

[13] R. Merrifield, Q. Long, X. Xu, P.J. Kilner, D.N. Firmin, G.Z. Yang, Combined cfd/mri analysis of left ventricular flow, Medical Imaging and Augmented Reality, Springer, 2004, pp. 229–236.

[14] V.T. Nguyen, S.N. Wibowo, Y.A. Leow, H.H. Nguyen, Z. Liang, H.L. Leo, A patient-specific computational fluid dynamic model for hemodynamic analysis of left ventricle diastolic dysfunctions, Cardiovascular Engineering and Technology 6 (2015) 412–429.

[15] N.R. Saber, A. Gosman, N.B. Wood, P.J. Kilner, C.L. Charrier, D.N. Firmin, Computational flow modeling of the left ventricle based on in vivo mri data: initial experience, Ann. Biomed. Eng. 29 (2001) 275–283.

[16] T. Schenkel, M. Malve, M. Reik, M. Markl, B. Jung, H. Oertel, MRI-based CFD analysis of flow in a human left ventricle: methodology and application to a healthy heart, Ann. Biomed. Eng. 37 (2009) 503–515.

[17] J.H. Seo, V. Vedula, T. Abraham, A.C. Lardo, F. Dawoud, H. Luo, R. Mittal, Effect of the mitral valve on diastolic flow patterns, Phys. Fluids 26 (2014).

[18] B. Su, R.S. Tan, J.L. Tan, K.W.Q. Guo, J.M. Zhang, S. Leng, X. Zhao, J.C. Allen, L. Zhong, Cardiac mri based numerical modeling of left ventricular fluid dynamics with mitral valve incorporated, J. Biomech. 49 (2016) 1199–1205.

[19] M. Gao, C. Chen, S. Zhang, Z. Qian, M. Vannan, S. Rinehart, D. Metaxas, L. Axel, Morphological analysis of the papillary muscles and the trabeculae, 2014 IEEE 11th International Symposium on Biomedical Imaging (ISBI), IEEE, 2014, pp. 373–376.

[20] S. Kulp, M. Gao, S. Zhang, Z. Qian, S. Voros, D. Metaxas, L. Axel, Using high resolution cardiac ct data to model and visualize patient-specific interactions between trabeculae and blood flow, Medical Image Computing and Computer-Assisted Intervention–MICCAI 2011 (2011) 468–475.

[21] S. Kulp, D. Metaxas, Z. Qian, S. Voros, L. Axel, V. Mihalef, Patient-specific modeling and visualization of blood flow through the heart, Biomedical Imaging: from Nano to Macro, 2011 IEEE International Symposium on, IEEE, 2011, pp. 1692–1697.

[22] J. Lantz, L. Henriksson, A. Persson, M. Karlsson, T. Ebbers, Patient-specific simulation of cardiac blood flow from high-resolution computed tomography, J. Biomech. Eng. 138 (2016) 121004.

[23] F. Sacco, B. Paun, O. Lehmkuhl, T.L. Iles, P.A. Iaizzo, G. Houzeaux, M. Vázquez, C. Butakoff, J. Aguado-Sierra, Left ventricular trabeculations decrease the wall shear stress and increase the intra-ventricular pressure drop in cfd simulations, Front. Physiol. 9 (2018) 458.

[24] V. Vedula, J.H. Seo, A.C. Lardo, R. Mittal, Effect of trabeculae and papillary muscles on the hemodynamics of the left ventricle, Theor. Comput. Fluid Dynam. 30 (2016) 3.

[25] F. Sacco, B. Paun, O. Lehmkuhl, T.L. Iles, P.A. Iaizzo, G. Houzeaux, M. Vázquez, C. Butakoff, J. Aguado-Sierra, Evaluating the roles of detailed endocardial structures on right ventricular haemodynamics by means of cfd simulations, International journal for numerical methods in biomedical engineering 34 (2018) e3115.

[26] A. Caballero, W. Mao, R. McKay, C. Primiano, S. Hashim, W. Sun, New insights into mitral heart valve prolapse after chordae rupture through fluid–structure interaction computational modeling, Sci. Rep. 8 (2018) 17306.

[27] V. Meschini, M.D. de Tullio, R. Verzicco, Effects of mitral chordae tendineae on the flow in the left heart ventricle, The European Physical Journal E 41 (2018) 27.

[28] S. Singh-Gryzbon, V. Sadri, M. Toma, E.L. Pierce, Z.A. Wei, A.P. Yoganathan, Development of a computational method for simulating tricuspid valve dynamics, Ann. Biomed. Eng. (2019) 1–13.

[29] C.S. Peskin, Numerical analysis of blood flow in the heart, J. Comput. Phys. 25 (1977) 220–252.

[30] C.S. Peskin, D.M. McQueen, Modeling prosthetic heart valves for numerical analysis of blood flow in the heart, J. Comput. Phys. 37 (1980) 113–132.

[31] M. Toma, D.R. Einstein, C.H. Bloodworth IV, R.P. Cochran, A.P. Yoganathan, K.S. Kunzelman, Fluid–structure interaction and structural analyses using a comprehensive mitral valve model with 3d chordal structure, Int. J. Numer. Methods Biomed. Eng. 33 (4) (2016) e2815.

[32] J.N. Sørensen, W.Z. Shen, Numerical modeling of wind turbine wakes, J. Fluids Eng. 124 (2002) 393–399.

[33] S.K. Dahl, E. Fagerholt, G. Kiss, V.E. Prot, B.H. Amundsen, L.R. Hellevik, B.H. Skallerud, 3d moving boundary conditions for heart cfd simulations - from echocardiographic recordings to discretized surfaces, MekIT'11: Sixth National Conference on Computational Mechanics, Tapir Akademisk Forlag, 2011, pp. 33–46.

[34] S.F. Hoerner, Fluid dynamic drag: practical information on aerodynamic and hydrodynamic resistance, SF Hoerner, Midland Park, New Jersey, USA, 1965.

[35] F.M. White, I. Corfield, Viscous Fluid Flow vol. 3, McGraw-Hill, New York, 2006.

[36] D. Sucker, H. Brauer, Investigation of the flow around transverse cylinders, Waerme und Stoffuebertragung 8 (1975) 149–158.

[37] Ansys Inc, ANSYS FLUENT Theory Guide, Release vol. 15, (Nov. 2013).

[38] J. Lam, N. Ranganathan, E. Wigle, M. Silver, Morphology of the human mitral valve i. chordae tendineae: a new classification, Circulation 41 (1970) 449–458.

[4] The drag coefficient based on Eq. (2) is larger than or of the order 1.